Available online at www.sciencedirect.com

SCIENCE DIRECT®

Journal of Molecular Catalysis A: Chemical 200 (2003) 323–332

JOURNAL OF MOLECULAR CATALYSIS A: CHEMICAL

www.elsevier.com/locate/molcata

Supported metallocene catalysts—interactions of $(n\text{-BuCp})_2HfCl_2$ with methylaluminoxane and silica

Nora I. Mäkelä-Vaarne [a,*], David G. Nicholson [b], Astrid Lund Ramstad [b]

[a] *Borealis Polymers Oy, R&D, P.O. Box 330, FIN-06101 Porvoo, Finland*

[b] *Department of Chemistry, Norwegian University of Science & Technology, Høgskoleringen 5, N-7491 Trondheim, Norway*

Received 23 October 2002; received in revised form 4 February 2003; accepted 4 February 2003

Abstract

The species on supported olefin polymerisation catalysts consisting of $(n\text{-BuCp})_2HfCl_2$, methylaluminoxane (MAO) and dehydroxylated silica were identified by EXAFS and UV-Vis spectroscopy. Whereas the reaction of $(n\text{-BuCp})_2HfCl_2$ with silica leads to a product containing Hf···O and Hf···Si non-bonded interactions with concurrent loss of Hf–Cl bonds, the reaction of $(n\text{-BuCp})_2HfCl_2$ with silica pretreated with methylaluminoxane yields a mixture of several hafnocene species. The bonding features of $(n\text{-BuCp})_2HfCl_2$ and $(n\text{-BuCp})_2HfCl_2/SiO_2$ are still present to some extent but with new interactions consistent with hafnocene cation formation. The relative proportions of these species depend strongly on the method of the catalyst preparation.

Keywords: EXAFS; UV-Vis; Hafnocene; Supported; Catalyst

1. Introduction

Catalysts based on metallocene complexes activated with methylaluminoxane (MAO) are a topic of extensive research (see, for example, the following reviews and references therein [1]). They exhibit high activities in olefin polymerisation and their single-site nature makes possible the synthesis of polymers with narrow molecular weight distributions and tailored microstructures. This is a significant advantage compared to conventional industrially-used heterogeneous Ziegler–Natta catalysts, the structures of which contain several different active sites.

On the face of it the paucity of information on the hafnocene systems prevents us from comparing the present data with those for other relevant hafnocene catalysts. Fortunately, this problem can be circumvented by comparing the hafnocene systems with the corresponding zirconocene ones because the lanthanide contraction makes the structures of zirconium ($[Kr]4d^25s^2$) and hafnium ($[Xe]4f^{14}5d^26s^2$) almost identical so that, for example, their radii (covalent and ionic (4+)) are virtually the same [2]. Chemical similarities of hafnium compounds are carried over into the corresponding zirconium compounds [3]. Since studies on zirconocene and hafnocene catalysts are heavily weighted (30:1) in favour of the former, we have transferred appropriate information on the zirconocene systems over to the corresponding hafnocene.

The majority of studies on catalyst active sites are on homogeneous systems. A number of different studies on homogeneous liquid phase zirconocene catalysts are consistent with the active site being $Cp_2Zr(CH_3)^+$

* Corresponding author.
E-mail address: nora.makela-vaarne@borealisgroup.com (N.I. Mäkelä-Vaarne).

1381-1169/03/$ – see front matter © 2003 Elsevier Science B.V. All rights reserved.
doi:10.1016/S1381-1169(03)00119-5

[4]. Current polymerisation technologies are mostly based on gas phase and slurry processes in which the role of the catalyst is to produce polymer particles with the desired morphology. This is facilitated by attaching the metallocene to a support. The choice of support is dictated by specific requirements; the material should be of low reactivity with respect to catalyst deactivation but at the same time sufficiently reactive to prevent leaching by attaching itself to the catalyst. The support exerts both positive and negative effects on catalyst behaviour. The most commonly used support material is partially dehydroxylated porous silica. Generally, the activities of supported metallocene catalysts are lower towards olefin polymerisation than in the corresponding homogeneous liquid phase systems because the diffusion of monomer into the pores of the catalyst is slower and the number of active centres reduced [5]. In the case of the zirconocene systems, the contrast between the unsupported and supported catalysts is illustrated by their different requirements for the activator MAO. Thus, whereas a large excess of MAO (i.e. [Al]/[Zr] $>$ 1000) is necessary for the unsupported catalyst, considerably smaller amounts (i.e. [Al]/[Zr] between 50 and 300) suffice for supported systems with similar activities [6]. It has been suggested that bimolecular deactivation is reduced in the supported systems relative to the homogeneous catalysts [7].

Despite the industrial interest in these catalysts, only a few studies on the species formed from reactions between the support, the metallocene and MAO have been reported. These studies focus mainly on the reactions and interactions between silica and metallocene [8] and not on the complete catalyst system (i.e. metallocene, MAO and silica). Rutherford back scattering and FTIR spectroscopy show that when (n-BuCp)$_2$ZrCl$_2$ reacts with dehydroxylated silica the concentration of hydroxyl groups on the silica support steers the reaction of zirconocene and thus the release of chloride ions in either a mono- or a bidentate way [9]. Species formed by the former mechanism are active in olefin polymerisation whilst those generated via the latter are inactive. In that work [9] MAO was added to the polymerisation reactor and not to the catalyst. In another study [10] X-ray photoelectron spectroscopy (XPS) shows the presence of two types of ion pairs, one assumed to be [SiO]$^-$[Et(Ind)$_2$ZrCl]$^+$ and the other a trapped multi co-ordinated crown complex of [Et(Ind)$_2$ZrCl]$^+$ and MAO$^-$. It was found that the ratio of the two species depends on the method used to prepare the heterogeneous system and the effect of omitting MAO leads to the sole product being the former cation. When *rac*-ethylenebis(1-indenyl)zirconium dichloride is immobilised on the surface of mesoporous silica and then modified with MAO, the EXAFS of the resulting system shows that the bonds between the metal and chloride ligands are broken, but with the indenyl ligand framework remaining intact and that there is a Zr–C bond consistent with the Zr$^+$-CH$_3$ fragment [11].

There are differences in behaviour between catalysts pretreated with MAO and the unpretreated ones. When the metallocene is supported on dehydroxylated silica pretreated with MAO, stereochemical analyses of the polypropylene produced show that the product profile is very similar to that obtained when using the homogeneous catalyst. This is consistent with the active sites in the homogeneous and heterogeneous systems being similar. However, catalytic activity is significantly reduced when the metallocene is first supported on dehydroxylated silica and subsequently activated in the polymerisation reactor with MAO; the polypropylene exhibits a markedly different microstructure [12]. From these studies it is clear that the preparation of the supported catalysts and the pre-treatment of silica determines the nature of the catalytically active species. This conclusion is of industrial and economic significance because the active species dictates the behaviour of the catalyst in the olefin polymerisation process.

Whereas previous work mainly concentrated on the zirconocene-based catalysts, this investigation focuses on the relatively little-studied hafnocene-based catalyst systems. The hafnocene (n-BuCp)$_2$HfCl$_2$ was chosen because it is a highly active catalyst in olefin polymerisation (our test polymerisation studies show that (n-BuCp)$_2$HfCl$_2$ activated with MAO and supported on silica has roughly 2/3 of the activity of corresponding zirconocene complex). The same conclusion was drawn in reference [13]. To shed more light on the nature of the active species on the supported activated metallocene catalysts and the effects of different preparative procedures, we report here an EXAFS and UV-Vis spectroscopic study on hafnocene-based catalysts.

2. Experimental

2.1. Catalyst preparation

The drying and storage of all chemicals and the preparation and handling of the catalysts was carried out under dry nitrogen. The hafnocene complex $(n\text{-BuCp})_2HfCl_2$ was purchased from Witco (purity checked by ^1H NMR), and methylaluminoxane (30 wt.%) (MAO) in toluene from Albemarle was used as the activator. The trimethylaluminium (TMA) content of MAO was given to be 4.9 wt.%. Dehydroxylated non-commercial silica from Grace Davison was used as the support. The silica was purchased in the dehydroxylated form. ^1H MAS NMR measurements showed that the silica contains 590 μmol isolated Si-OH/g silica, 150 μmol H-bonded Si-OH/g silica. Bound water was not found. The surface area of the silica is 296 m^2/g, average pore diameter 20.9 nm and pore volume 1.5 ml/g, according to BET analysis. The samples were analysed for hafnium and aluminum content (wt.%) using a Thermo Elemental Iris Advantage XUV ICP-AES spectrometer.

2.1.1. Preparation of sample 3

The hafnocene complex was added as a fine powder to the support and heated whilst being mixed for 2 h at 80 °C.

2.1.2. Preparation of sample 4

(a) Silica was weighed under dry nitrogen into a glass bottle equipped with a magnetic stirrer and a slurry was formed by adding a toluene solution of MAO. After mixing for 2 h at room temperature, the excess solvent was evaporated by gentle heating (50 °C) under nitrogen. This gave 10.3 wt.% aluminium concentration in the silica (ICP). (b) The hafnocene complex was added as a fine powder to the dried MAO-treated support and heated whilst being mixed (2 h at 80 °C) yielding a product with an [Al]/[Hf] ratio of 167.

2.1.3. Preparation of sample 5

MAO and $(n\text{-BuCp})_2HfCl_2$ were first dissolved in toluene, the solution added to the silica under stirring and the resulting slurry allowed to react for 2 h under nitrogen at room temperature. Excess solvent was evaporated by cautious heating (50 °C) under nitrogen to give a catalyst with 6.5 wt.% aluminium and [Al]/[Hf] ratio of 204 (ICP).

The hafnium contents of the materials studied, and their designations are listed in Table 1 with a schematic summary of the preparative routes being shown in Fig. 1.

Table 1
The studied samples

Sample	Components	Hf content (wt.%)
1	SiO_2	0
2	$(n\text{-BuCp})_2HfCl_2$	36.29
3	1 g SiO_2 + 15 mg $(n\text{-BuCp})_2HfCl_2$	0.54
4	1 g SiO_2 + 2.5 ml 30% MAO + 15 mg $(n\text{-BuCp})_2HfCl_2$	0.41
5	2.5 ml 30% MAO + 12 mg $(n\text{-BuCp})_2HfCl_2$ + 2 g SiO_2	0.21

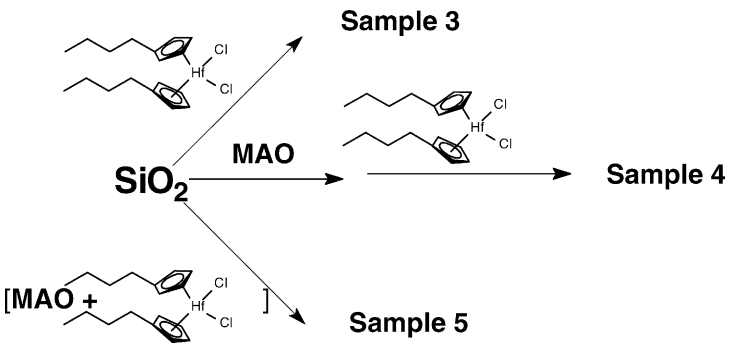

Fig. 1. Summary of the preparative routes.

2.2. XAS measurements

XAS data were collected using the facilities of the Swiss–Norwegian Beamline (SNBL) at the European Synchrotron Radiation Facility (ESRF), France. All spectra were measured at room temperature. Samples were placed in quartz capillaries (2 mm diameter) the operations being carried out in a glove box under dry nitrogen. The open ends of the capillaries were sealed with dried vacuum grease. Except for the reference compound ((*n*-BuCp)$_2$HfCl$_2$, which was sealed in a standard EXAFS holder with kapton windows), all of the samples were presented to the beam in this manner. Vacuum-dried boron nitride was used to dilute the (*n*-BuCp)$_2$HfCl$_2$ complex (volume ratio 5:1) in order to carry out the measurements in the fluorescence mode. (For thin capillaries the fluorescence mode is less sensitive than the transmission mode to any variations in incident beam position.) For air-sensitive materials, it is crucial to establish that degradation of the samples has not occurred during any stage of the data collection. Accordingly, the first and final scans for each sample had to be consistent before all of the spectra for that sample were summed. This procedure for air-sensitive materials has been carried out successfully by us in previous work [14].

The measurements were carried out at the hafnium L_{III} edge (9569 eV). A channel-cut Si(III) monochromator with an unfocussed beam was used to scan the X-ray spectra. Beam currents ranged from 130 mA to 200 mA at 6.0 GeV. Higher-order harmonics were rejected by means of a chromium-coated mirror angled at 3.3 mrad to give a cut-off energy of approximately 16 keV.

The maximum resolution $\Delta E/E$ of the Si(1 1 1) bandpass is 1.4×10^{-4} using a beam of size 0.6 mm × 7.2 mm as defined by the slits in the station. Ion chamber detectors with their gases at ambient pressures were used for measuring the intensities of the incident (I_0), transmitted (I_t), and fluorescent (I_f) X-rays. The detector gases were as follows: I_0, detector length 17 cm, 97% N_2, 3% Ar; I_t, length 31 cm, 50% N_2, 50% Ar; I_f (Lytle detector, see below), 100% Ar.

The fluorescent radiation was measured using a detector of the type developed by Lytle [15]. The signal:noise ratio was enhanced using a set of Soller slits and a Ni (three absorption lengths) filter. Due to the low metal content, nine scans were taken of each sample and summed. The energy calibration was checked by measuring the spectrum of a zinc foil (thickness 0.005 mm) with the energy of the first inflection point being defined as the edge energy.

2.3. EXAFS data analysis

The EXAFS data were formatted and corrected for dark currents, calibrated and summed and background subtracted to yield the EXAFS function by means of the Daresbury programs, EXCALIB and EXBACK, respectively [16]. Model fitting was carried out using the EXCURV98 program [17] using curved-wave theory and ab initio phase shifts calculated from within the program.

(*n*-BuCp)$_2$HfCl$_2$ (sample 2) was used as the reference compound for the unknown samples 3 and 4, to check the validity of the ab initio calculations and to establish the parameters AFAC (amplitude reduction due to many-electron processes) and VPI (energy-independent correction imaginary potential used to describe the lifetime of the electron) parameters [18]. These parameters were then transferred into the analyses of the unknowns in order to reduce any residual systematic error in the multiplicities. The EXAFS spectra were least square curved fitted using a k^0 and k^2-weighted data thereby reducing the coupling between N (multiplicity) and $2\sigma^2$ (Debye–Waller-type factor) by choosing solutions common to both weighting schemes [19].

2.4. UV-Vis spectroscopic measurements

In addition to the EXAFS experiments, UV-Vis spectroscopy was used as a complementary technique. The finely powdered samples were placed into quartz cells in a glove box filled with dry nitrogen; the cells were sealed with teflon stoppers. Spectra were measured in the reflectance mode using a Perkin-Elmer Lambda 900 spectrophotometer equipped with a diffuse reflectance integrating sphere. The scanning speed was 120 nm/min and data interval 2 nm. The spectrum was scanned over the range of 200–800 nm.

3. Results and discussion

A combination of EXAFS and UV-Vis spectroscopies was used to study the catalyst species at different stages of the different catalyst preparation routes.

3.1. EXAFS

The EXAFS results of samples 2 (used as a reference compound) and 3 are given in Table 2. The background subtracted k^2-weighted EXAFS spectra and the Fourier transforms are shown in Fig. 2.

3.2. Sample 2 ((n-BuCp)$_2$HfCl$_2$)

This hafnocene complex was used in the preparation of the samples identified in Fig. 1. In order to get the best possible reference for the bond lengths, several attempts were made to grow single crystals of (n-BuCp)$_2$HfCl$_2$. In all cases these were fruitless, leading only to powders unsuitable for X-ray crystal structure analysis. Since the crystal structure of this complex is not available, we resorted to carrying out the EXAFS analysis using structural parameters extracted from the literature [20–23] (i.e. Hf–Cp and Hf–Cl bond lengths 0.250 and 0.243 nm, respectively).

Two models were used to represent the n-BuCp rings; the first grouped together all 10 cyclopentadiene carbon atoms whereas the second partitioned them into a two plus eight (i.e. $2 \times (1 + 4)$) combination. No significant differences were obtained. Therefore, results of the first simpler parameter set are reported. The structural parameters derived from the EXAFS analysis on the reference complex are listed in Table 2.

An interesting feature in the EXAFS is the presence of a Hf$\cdots$Hf distance at 3.76 Å. The clearly visible peaks in the Fourier transform at 0.328 and 0.351 nm

Table 2
EXAFS results of (n-BuCp)$_2$HfCl$_2$ (sample 2, the reference compound) and (n-BuCp)$_2$HfCl$_2$/SiO$_2$ (sample 3, unknown)

Sample	Shell	Backscatter	N	R (nm)	(0.01) σ^2 (nm^2)	Assignment
2	1st	C	10[a]	0.2506 (9)	0.011 (11)	Cyclopentadienyl C
	2nd	Cl	2[b]	0.2444 (7)	0.003[c]	Cl
	3rd	C	4.0 (7)	0.3283 (15)	0.003[c]	n-Butyl C[d]
	4th	C	4.2 (8)	0.3512 (13)	0.002 (3)	n-Butyl C[d]
	5th	Hf	1.2 (4)	0.3762 (16)	0.006 (3)	Bridge[c,d]
3	1st	C	10[a]	0.2493 (7)	0.011 (2)	Cyclopentadienyl C
	2nd	Cl	1.6 (2)	0.2419 (9)	0.003[c]	Cl
	3rd	O	3.6 (5)	0.2796 (11)	0.003 (2)	O[d]
	4th	Si	7.0 (8)	0.3073 (11)	0.013 (3)	Si[d]
	5th	C	4.4 (12)	0.3450 (18)	0.002[c]	n-Butyl C
	6th	C	3.2 (15)	0.3831 (35)	0.003[c]	n-Butyl C
	7th	Hf	1.5 (9)	0.38551 (32)	0.011 (5)	Hf interaction[d]

N: multiplicity, R: interatomic distance and σ^2: Debye–Waller factor: root mean square deviation of the interatomic distance about R. Note that systematic errors in multiplicity and bond distances arising from data collection and analysis are ±20% and ±0.002–0.003 nm for well-defined shells, respectively.

$$R_{\mathrm{EXAFS}}\text{-factor},\ R_{\mathrm{EXAFS}} = \left\{ \frac{\sum_i^N [(\chi_{\mathrm{obs}} - \chi_{\mathrm{calc}}) k_i^{\mathrm{WT}}]^2}{\sum_i^N [\chi_{\mathrm{obs}} k_i^{\mathrm{WT}}]^2} \right\} \times 100\%$$

where N is the number of data points, WT the integral weighting, and χ_{obs} and χ_{calc} are the observed and calculated EXAFS, respectively. Sample 2: $R_{\mathrm{EXAFS}} = 30.07\%$, Sample 3: $R_{\mathrm{EXAFS}} = 36.51\%$.

[a] Not refined, kept at literature mean values (2Cp rings).
[b] Not refined, kept at literature values (2Cl atoms).
[c] Not refined.
[d] Non-bonded interactions.

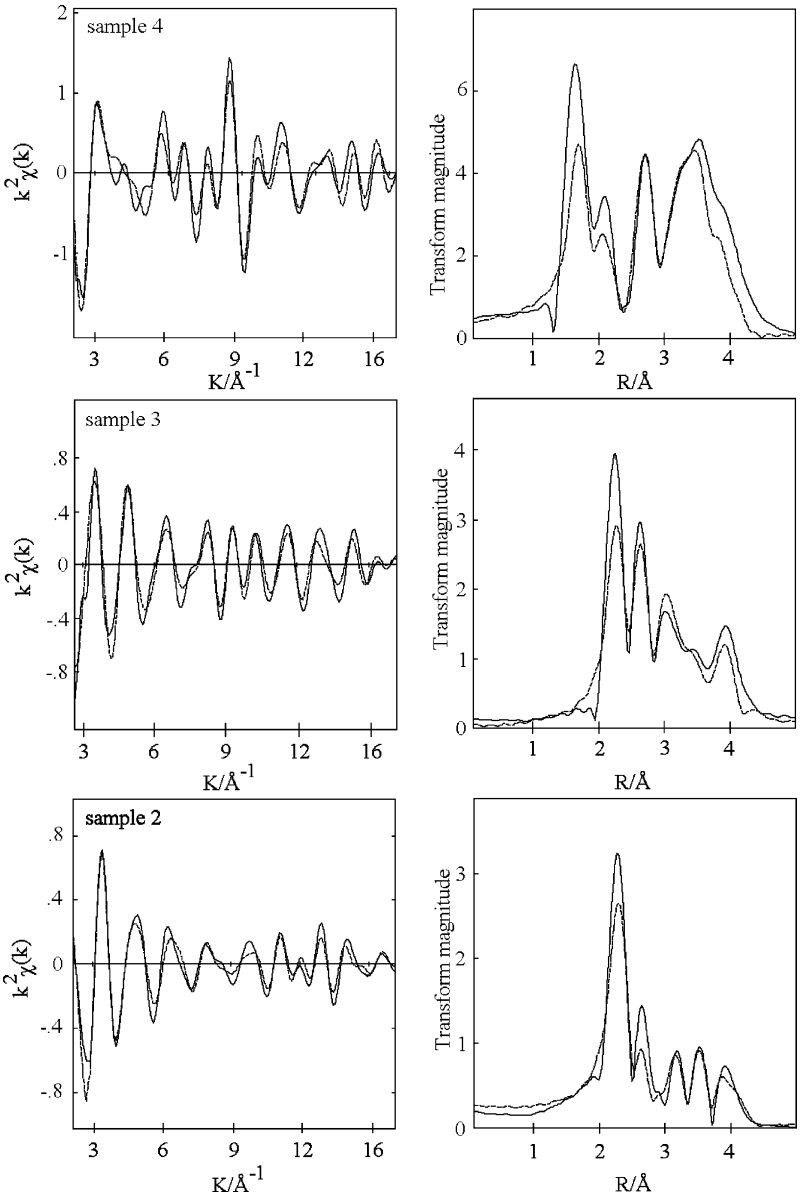

Fig. 2. Background subtracted k^2-weighted EXAFS spectra ((—) experimental and (---) calculated) and their Fourier transforms for the Hf supported catalysts, Hf L_{III}-edge: sample 2 ((*n*-BuCp)$_2$HfCl$_2$), sample 3 ((*n*-BuCp)$_2$HfCl$_2$/SiO$_2$) and sample 4 ((*n*-BuCp)$_2$HfCl$_2$/SiO$_2$/MAO), (1 Å = 0.1 nm).

are attributed to the carbon atoms in the *n*-butyl fragments. This result accords with molecular modeling simulations (semi-empirical, PM3 calculations) [24] that we used as an aid in the interpretation of these EXAFS results.

3.3. Sample 3 ((n-BuCp)$_2$HfCl$_2$/SiO$_2$)

Two additional interactions were found in the reaction product formed from the hafnocene complex and dehydroxylated silica. The 3rd and 4th shells

are assigned to silica–hafnocene distances via oxygen non-bonded interactions. The Fourier peak at 0.307 nm is attributed to a composite of different Hf···Si non-bonded distances that is reflected by the multiplicity (Table 2). The EXAFS analysis also includes interactions from the *n*-butyl groups. Interactions between hafnium and the *n*-butyl carbon atoms are given at mean values. As is the case for sample 2, these distances (0.345 nm and 0.383 nm) are consistent with the molecular modelling simulations (see above).

The EXAFS shows a reduced Hf–Cl contribution to the overall spectrum which suggests that a significant fraction (approximately 50%) of the $(n\text{-BuCp})_2HfCl_2$ has reacted with silica, thereby losing one chlorine atom and leading to a composite EXAFS spectrum. The resulting monochloride species has been observed earlier for the zirconocene–silica system and was concluded to be cationic [10]. UV-Vis spectroscopy (Fig. 4) reveals that sample 3 does not include significant amounts of unreacted $(n\text{-BuCp})_2HfCl_2$, instead at least two additional species absorbing at visible range (450 nm and 570 nm) are present. As mentioned above, we expect $-Si-O^- -^+Hf(Cl)(n\text{-BuCp})_2$ species to be present and they could be the origin of one of the two bands observed in UV-Vis spectrum. In addition to these species, we expect that the $(n\text{-BuCp})_2HfCl_2$ interacts with the silica oxygens in non-bonded ways, and that these interactions can be seen as another broad band in the UV-Vis spectrum. EXAFS shows an average (0.280 nm) of four Hf···O distances. It is clear from the Fourier transform that there is not a Hf···SiO_2 distance within the range 0.18–0.21 nm that would indicate a Hf–O covalent bond. This is interesting and presumably can be rationalised in terms of steric hindrance.

The Hf···Hf distance (0.376 nm) present in sample 2, is somewhat longer (0.386 nm) in sample 3. The presence of Hf···Hf interactions in this sample is consistent with the method of preparation in which the hafnocene dichloride was added as a finely dispersed powder on silica. Hence, the hafnocene molecules are close enough to interact with each other.

These results show that in sample 3 approximately 50% of the hafnocene has reacted by losing a Cl atom with the remainder of the hafnocene interacting with the silica surface in a non-bonded way.

3.3.1. Sample 4 ($(n\text{-BuCp})_2HfCl_2/SiO_2/MAO$)

Fig. 3 compares the k^2-weighted EXAFS spectrum of sample 4 with the spectra of samples 2 and 3.

There are noticeable differences between the EXAFS of samples 3 and 4 with the latter showing the effects of interference consistent with different hafnium environments and (as already mentioned) interactions with the support. This means that the spectrum of sample 4 is a composite due to the material being actually a mixture of several hafnium-containing phases. For this reason the structural parameters are not included in Table 2. Although this is consistent with the XPS results [10] (see above) in that ion pairs are detected, the EXAFS actually appears more consistent with there being more than the two hafnocene cations found by XPS.

The UV-Vis absorption spectrum (Fig. 4) shows that a significant fraction of unreacted hafnocene is present in the catalyst (sample 4). In sample 3 we could see only a negligible part of unreacted $(n\text{-BuCp})_2HfCl_2$ in UV-Vis spectrum. This is interesting because the difference between the two samples lies in the method of preparation. The preparation of sample 4 includes MAO at the surface of the silica and in sample 3 $(n\text{-BuCp})_2HfCl_2$ is added on pure dehydroxylated silica. In sample 4 a significant fraction of the hafnocene remains unreacted, i.e the reaction of hafnocene was less efficient with silica pretreated with MAO than with pure silica.

3.3.2. Sample 5($(n\text{-BuCp})_2HfCl_2/SiO_2/MAO$)

Since the hafnium concentration of sample 5 was too low to give a good quality EXAFS, the spectrum was not analysed (Table 1).

UV-Vis spectroscopy was used to study the species on the silica support thereby complementing the EXAFS experiments. This technique has been used earlier to study electronic structures of zirconocenes [24] and zirconocene activation [4]. In the metallocene studies the band of most interest is due to the ligand-to-metal charge transfer (LMCT) transition since it is sensitive to changes in the environment about the metal such as ligand changes.

LMCT transitions usually occur in the visible range and in the case of the zirconocenes arise from the charge transition from the HOMO associated with the cyclopentadienyl ligand to d^0 Zr-based LUMO [25]. Fig. 4 shows the UV-Vis absorption spectra

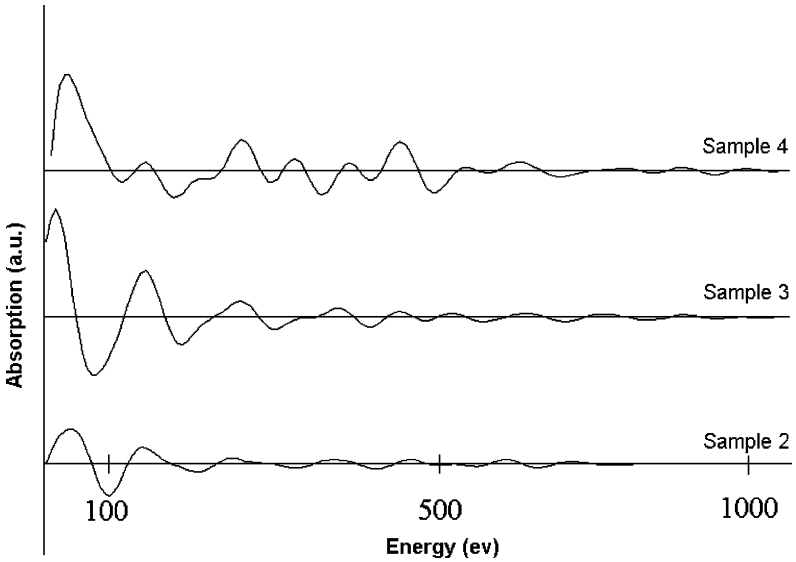

Fig. 3. Experimental k^2-weighted EXAFS spectra for sample 2 ((*n*-BuCp)$_2$HfCl$_2$), sample 3 ((*n*-BuCp)$_2$HfCl$_2$/SiO$_2$) and sample 4 ((*n*-BuCp)$_2$HfCl$_2$/SiO$_2$MAO).

of the samples. Pure dehydroxylated silica absorbs in UV range at around 240 nm (sample 1). When the hafnocene complex is added to this material the absorption properties change drastically (sample 3). Two new absorptions appear at 450 nm and 570 nm. These absorptions were absent in the spectrum of the sample 2 (the pure complex). The 315 nm absorption in the sample 2 is assigned to the LMCT transition: *n*-BuCp (HOMO) to Hf (LUMO). The absorption at 300 nm is being assigned to the $\pi \rightarrow \pi^*$ transitions within the cyclopentadienyl ligand. Hence, the absorptions of sample 3 (450 nm and 570 nm) are assigned to silica–hafnocene interactions found also by the EXAFS (see above).

In the UV-Vis studies on homogeneous metallocene catalysts, metallocene cationisation is manifested by a

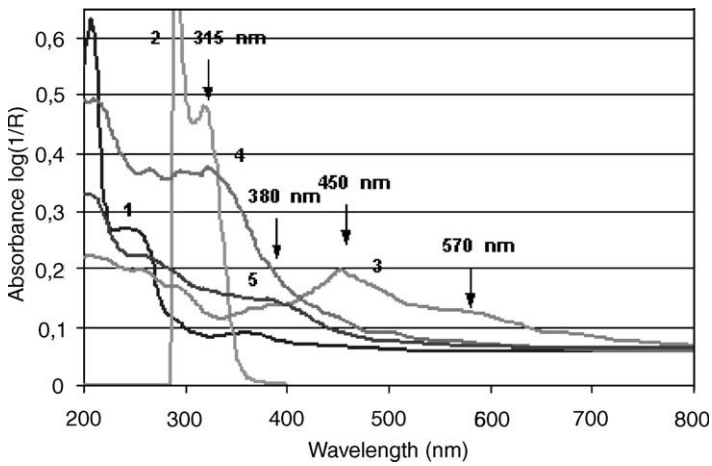

Fig. 4. Normalised UV-Vis spectra of samples 1–5.

shift in the LMCT band to lower energies, i.e. to higher wavelengths. MAO reacts with $(n\text{-BuCp})_2HfCl_2$ by abstracting the chloride ions and replacing them with one methyl group and a positive charge. This further decreases the electron density at the hafnium atom which leads to a concomitant decrease in the energy of the LMCT because electron density is more easily transferred from the electron-rich cyclopentadienyl ligands to the electron-poor metal. Such a band shift was also observed for the supported catalyst studied here. The appearance of a shoulder on the broad band at around 380 nm would be consistent with the hafnocene monomethyl–MAO ion pairs. However, the breadth of this band is consistent with the presence of more than one type of cationic hafnocene species.

The bands at 450 nm and 570 nm, revealing silica–hafnocene interaction, were too low to be detected when the catalyst was prepared by pretreating silica with MAO prior to adding hafnocene (sample 4). This indicates a reduction in the direct non-bonding interactions between silica and hafnocene, as one could expect. Unreacted hafnocene was concluded to be present in sample 4 since the absorption at 315 nm due to hafnocene is still visible. This applies more to the sample 4 than sample 5 since in sample 5, in which hafnocene was allowed to react with MAO prior to addition on silica, the 315 nm band is negligible. MAO itself absorbs at 290–300 nm and can partially cover the contribution of the 300 nm band of pure dichloride complex.

4. Conclusions

EXAFS and UV-Vis spectroscopy were used to resolve different species present in $(n\text{-BuCp})_2HfCl_2$-based catalysts. For the hafnocene $(n\text{-BuCp})_2HfCl_2$ EXAFS showed the presence of a Hf···Hf interaction and a Hf···*n*-butyl distance, in addition to the expected Hf–Cp and Hf–Cl interactions. $(n\text{-BuCp})_2HfCl_2$ reacts with silica to produce two additional non-bonding interactions, namely Hf···Si and Hf···O. A composite EXAFS spectrum was obtained in the case of the catalyst prepared by pretreating silica with MAO prior adding the hafnocene. The spectrum consisted of unreacted hafnocene and low concentrations of hafnocene–silica species. Furthermore, additional spectral features revealing different cationised hafnocene species were present. UV-Vis spectroscopy supported the EXAFS results by also showing the presence of unreacted hafnocene species. A higher contribution of the cationised hafnocene species in the UV-Vis spectrum was observed for the catalyst prepared by allowing MAO to react with $(n\text{-BuCp})_2HfCl_2$ before adding to silica.

Acknowledgements

Financial support from the Faculty of Natural Science and Technology, Norwegian University of Science and Technology and the Norwegian Research Council is much appreciated. Experimental assistance from the staff (W. Van Beck, H. Emerich, P. Pattison and H.P. Weber) of the Swiss–Norwegian Beam Lines at ESRF is gratefully acknowledged. Fortum analytical laboratory is thanked for the BET and ^1H MAS NMR measurements of silica. We also thank Mr. Jouni Hoikka for assistance with the computer modelling and Ms. Ritva Lindfors for carrying out the elemental analyses and Ms. Inge Sahlberg for preparing the catalysts.

References

[1] (a) P.C. Möhring, N.J. Coville, J. Organomet. Chem. 479 (1994) 1;
(b) H.H. Brintzinger, D. Fischer, R. Mülhaupt, B. Rieger, R.M. Waymouth, Angew. Chem. Int. Ed. Engl. 34 (1995) 1143;
(c) W. Kaminsky, Macromol. Chem. Phys. 197 (1996) 3907;
(d) W. Kaminsky, M. Arndt, Adv. Polym. Sci. 127 (1997) 143;
(e) C. Janiak, in: A. Togni, R.L. Halterman (Eds.), Metallocenes: Synthesis, Reactivity, Applications; Wiley–VCH, Weinheim, Germany, 1998;
(f) G.G. Hlatky, Chem. Rev. 100 (2000) 1347.

[2] F.A. Cotton, G. Wilkinson, C.A. Murillo, M. Bochmann (Eds.), Advanced Inorganic Chemistry, sixth ed., Wiley/Interscience, New York, 1999, pp. 878–895.

[3] N.N. Greenwood, A. Earnshaw (Eds.), Chemistry of the Elements, second ed., Butterworth Heinemann, London, 1997, pp. 972–975.

[4] (a) N.I. Mäkelä, H.R. Knuuttila, M. Linnolahti, T. Pakkanen, M. Leskelä, Macromolecules 35 (2002) 3395;
(b) D. Coevoet, H. Cramail, A. Deffieux, Macromol. Chem. Phys. 199 (1998) 1451;
(c) J.A.M. van Beek, P.J.J. Pieters, M.F.H. van Tol, in: Proceedings of the Metallocenes'95, Brussels, April 26–27, 1995;

(d) U. Wieser, H.H. Brintzinger, in: R. Blom, A. Follestad, E. Rytter, M. Tilset, M. Ystenes (Eds.), Organometallic Catalysts and Olefin Polymerisation: Catalysts for a New Millenium, Springer, 2001;
(e) D.E. Babushkin, N.V. Semikolenova, V.A. Zakharov, E.P. Talsi, Macromol. Chem. Phys. 201 (2000) 558;
(f) P.G. Gassman, R. Callstrom, J. Am. Chem. Soc. 109 (1987) 7875;
(g) I. Tritto, R. Donetti, M.C. Sacchi, P. Locatelli, G. Zannoni, Macromolecules 30 (1997) 1247;
(h) C. Sishta, R.M. Hathorn, T.J. Marks, J. Am. Chem. Soc. 114 (1992) 1112;
(i) M. Linnolahti, T. Pakkanen, Macromolecules 33 (2000) 9205;
(j) P.A. Deck, T.J. Marks, J. Am. Chem. Soc. 117 (1995) 6128.

[5] (a) T.J. Marks, J.C. Stevens (Eds.), Topics in Catalysis, vol. 7, Baltzer, Amsterdam, 1999, pp. 23–36;
(b) P.J.T. Tait, M.G. Monteiro, M. Yang, J.L. Richardson, in: Proceedings of the MetCon 1996, Houston, Texas.

[6] (a) J.C.W. Chien, D. He, J. Polym. Sci. Polym. Chem. 29 (1991) 1603;
(b) W. Kaminsky, Macromol. Symp. 97 (1995) 79.

[7] A. Patchornik, M.A. Kraus, J. Am. Chem. Soc. 92 (1970) 7587.

[8] (a) M. Jezequel, V. Dufayd, J. Ruiz-Garzia, F. Carrillo-Hermosilla, U. Neugebauer, G. Niccolai, F. Lefebvre, F. Bayard, J. Corker, S. Fiddy, J. Evans, J. Broyer, J. Malinge, J. Basset, J. Am. Chem. Soc. 123 (2001) 3520;
(b) M. Kröger-Laukkanen, M. Peussa, M. Leskelä, L. Niinistö, Appl. Surf. Sci. 183 (2001) 290.

[9] (a) J.H.Z. Dos Santos, C. Krug, M.B. da Rosa, F.C. Stedile, J. Dupont, M. Forte, C. J. Mol. Catal. A: Chem. 139 (1999) 199;
(b) F.C. Stedile, J.H.Z. Dos Santos, Phys. Status Solidi A 173 (1999) 123.

[10] M. Atiqullah, M. Faiz, M.N. Akhtar, M.A. Salim, S. Ahmed, J.H. Khan, Surf. Interface Anal. 27 (1999) 728.

[11] S. O'Brien, J. Tudor, T. Maschmeyer, D. O'Hare, Chem. Commun. (1997) 1905.

[12] (a) M.C. Sacchi, D. Zucchi, I. Tritto, P. Locatelli, T. Dall'Occo, Macromol. Rapid Commun. 16 (1995) 581;
(b) W. Kaminsky, F. Renner, Macromol. Chem. Rapid Commun. 14 (1993) 239.

[13] D.T. Mallin, M.D. Rausch, J.C.W. Chien, Polym. Bull. 20 (1988) 421.

[14] M. Rønning, T. Gjervan, R. Prestvik, D. Nicholson, A. Holmen, J. Catal. 204 (2001) 292.

[15] F.W. Lytle, Nucl. Instrm. Methods Phys. Res. 226 (1984) 542.

[16] N. Binstead, J.W. Campbell, S.J. Gurman, P.C. Stephenson, EXCALIB and EXBACK programs, SERC Daresbury Laboratory, 1990.

[17] N. Binstead, J.W. Campbell, S.J. Gurman, P.C. Stephenson, EXCURV98 program, SERC Daresbury Laboratory, 1998.

[18] S.J. Gurman, N. Binsted, I. Ross, J. Phys. C 17 (1984) 143.

[19] F.W.H. Kampers, C.W.R. Engelen, J.H.C. Van Hooff, D.C. Konigsberger, J. Phys. Chem. 94 (1990) 8574.

[20] W.E. Hunter, D.C. Hrncir, R.V. Bynum, R.A. Penttila, J.L. Atwood, Organometallics 2 (1983) 750.

[21] S.L. Buchwald, K.A. Kreutzer, R.A. Fisher, J. Am. Chem. Soc. 112 (1990) 4600.

[22] (a) T. Repo, M. Klinga, I. Mutikainen, Y. Su, M. Leskelä, M. Polamo, Acta Chim. Scand. 50 (1996) 1116;
(b) R.A. Howie, G.P. McQuillan, D.W. Thompson, G.A. Lock, J. Organomet. Chem. 303 (1986) 213.

[23] T.N. Doman, T.K. Hollis, B. Bosnich, J. Am. Chem. Soc., 117 (1995) 1352.

[24] PC Spartan Pro, Wavefunction Inc.

[25] (a) N.I. Mäkelä, H.R. Knuuttila, M. Linnolahti, T.A. Pakkanen, J. Chem. Soc., Dalton Trans. 1 (2001) 91;
(b) U. Wieser, F. Schaper, H.H. Brintzinger, N.I. Mäkelä, H.R. Knuuttila, M. Leskelä, Organometallics 21 (2002) 541.